

Vertex Simulation of Grain Growth from Electron Backscatter Diffraction Data

N. MAAZI*

Laboratoire Microstructures et Défauts dans les Matériaux (LMDM), Département de Physique, Faculté des Sciences Exactes, Université Mentouri Constantine 1, 25000 Constantine, Algeria

Received: 12.10.2021 & Accepted: 03.02.2022

Doi: [10.12693/APhysPolA.141.467](https://doi.org/10.12693/APhysPolA.141.467)

*e-mail: nmaazi@yahoo.fr

Vertex method to simulate grain growth usually starts with the use of a homogeneous theoretical microstructure obtained by Voronoi tessellation. This microstructure does not represent real materials where the grains are not homogeneously distributed in terms of size and orientation. In order to take into account these inhomogeneities, and consequently correctly describe the grain growth process, in this paper a vertex simulation begins with the use of the experimental microstructure as the initial data. To facilitate the simulation procedure as well as the analysis of the result, instead of using only the network of grain boundaries and vertices to represent the microstructure in the standard vertex model, we use a hexagonal lattice to discretize the physical space. Each site of the hexagonal lattice is assigned three Euler angles that represent the grain orientation at that lattice site.

topics: EBSD, hexagonal lattice, vertex simulation, grain growth

1. Introduction

The properties of polycrystalline materials are directly related to their microstructures. The anisotropic properties of materials are due to the morphological and textural inhomogeneities of the microstructure, which result from the grain growth process at the mesoscopic level. The grains evolution is governed by the migration of grain boundaries (GBs) towards their center of curvature [1]. Consequently, the boundary in the two-dimensional grain structure decreases its length during grain growth, and the average grain size \bar{R} increases by eliminating small grains.

Various computer models have been used to simulate grain growth in polycrystalline materials, which include vertex [2–4], Monte Carlo (MC) Potts [5–7], cellular automata [8, 9], and phase field [10, 11]. Grain growth at the mesoscopic scale is usually studied using stochastic MC and deterministic vertex models. On the one hand, owing to the simplicity and flexibility of implementing the MC method, it is widely used to simulate several aspects of the grain growth process. The strength of this technique results from the easy way the microstructure is represented. On the other hand, although the vertex technique is based on the physical principles and is an efficient way to study the grain growth phenomena, there are some obstacles to this technique. Its limitations result from the cost of the

high computational complexity of representing of the microstructure in the standard vertex simulation. For example, topological events such as grain shrinkage are difficult to manage during the grain growth process. The grain boundary networks and the vertices (triple points), at which these boundaries intersect, represent the microstructure. The grains are defined by the collection of boundaries and the triple junctions surrounding them. Their area is not discretized.

The vertex model has been used in different simulation of microstructural evolution such as: recrystallization [12, 13], normal grain growth [4, 14], abnormal grain growth [15], and also grain growth in the presence of the Zener pinning effect [16]. The morphological and textural inhomogeneities of the microstructure play an important role in the grain growth process at mesoscopic level. Because of the complexity of the task, the vertex model does not make attention to the neighbourhood of individual grains. With important progress of electron backscatter diffraction (EBSD) technology [17], it has become possible to directly use experimental microstructures measured by orientation imaging microscopy (OIMTM) [18] to start the simulation especially for the Monte Carlo technique. Therefore, a call was made to develop a standard vertex technique that enables the full use of EBSD data. Modifications in the framework of the vertex model are suggested in the present work, where the grain's

area is discretized. The vertex model is laid on top of a fixed hexagonal lattice that stores the grain orientation data. Neighbouring points with the same orientation define the grains. The interface lines between neighbouring points of different orientations represent GBs. Triple points are automatically represented. In the simulation procedure, a new definition for the critical size is given to start the topological transformations T1 and T2. These modifications permit for an easy start of simulation using experimental microstructure.

2. Vertex method of grain growth simulation

In basic vertex models, grains are always limited by straight edges [2, 3]. During the simulation procedure, the motion of the triple junctions (real vertices) exclusively controls the minimization of the free energy of the system. As a result, no driving forces are associated with the grain boundary curvature. In these models, the driving forces for grain growth are the grain boundary tensions acting upon the triple junctions. However, these vertices move in the direction of the resultant tensions with velocity vector

$$\mathbf{v}_i = m_i \sum_{j=1}^3 \sigma_{ij} \frac{\mathbf{r}_{ij}}{|\mathbf{r}_{ij}|}, \quad (1)$$

where m_i [$\text{m}^2/(\text{J s})$] is the mobility of the vertex i , σ_{ij} [J/m] is the energy per unit length of grain boundary between the triple points i and j , and \mathbf{r}_{ij} is the vector connections point i to the point j .

To consider the driving forces resulting from the curvature of the grain boundaries, the lines between the two triple junctions are discretized by the so-called virtual vertices (double junctions) [19, 20]. At the grain boundary, the virtual vertex is connected to the two nearest neighbouring vertices. Such vertices permit the calculation of the local curvatures of the grain boundaries. In each time increment Δt , the boundary segments or virtual vertices move perpendicularly to the boundary line with velocity

$$v_i = m_{gb} \sigma_{gb} \rho_i, \quad (2)$$

where m_{gb} [$\text{m}^2/(\text{J s})$] and σ_{gb} [J] are the grain boundary mobility and energy of the grain, respectively, and ρ_i [m^{-1}] is the local grain boundary curvature at virtual vertex i .

The new positions of the vertices are calculated from the following relation

$$\mathbf{r}_i(t + \Delta t) = \mathbf{r}_i(t) + \mathbf{v}_i(t) \Delta t. \quad (3)$$

The velocities of the vertices $\mathbf{v}_i(t)$ are obtained from (1) and (2).

The kinetics of normal grain growth is governed by increasing the average grain size \bar{R} according to [21]

$$\bar{R}^2 - \bar{R}_0^2 = kt, \quad (4)$$

where k [m^2/s] is a constant and \bar{R}_0 [m] is the initial average grain size at $t = 0$.

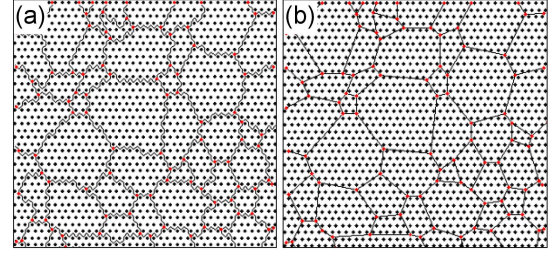


Fig. 1. Real microstructure (a) and the corresponding network of lines (b). Red points represent triple points.

In two dimensions, von Neumann and Mullins [22, 23] showed that the rate of the growth of n -sided grain is

$$\frac{dA}{dt} = \frac{\pi}{3} m_{gb} \sigma_{gb} (n - 6), \quad (5)$$

where A [m^2] is the area of the grain. A grain with $n > 6$ will grow, whereas a grain with $n < 6$ will shrink.

3. Development of a standard vertex method

In the vertex model, the initial microstructure is constructed using Voronoi tessellation. The real and virtual vertices (triple and double junctions respectively) represent the grain structure. Because of the complexity of this representation, few works have used this method in comparison on other methods, e.g. MC technique. In the vertex model only the grain boundary is discretized, but the grain interior is not; however no assumptions are made about the shape, size or neighborhood of individual grains in the vertex model. On the other hand, the use of a homogeneous theoretical microstructure obtained by Voronoi tessellation is not representative of real materials in which the grains are not homogeneously distributed in terms of sizes and orientations. In the present work, first, in order to take into account morphological and textural inhomogeneities and, consequently, to correctly describe the grain growth process, the simulation is started by using the experimental microstructure as initial data. In this case, it is not required to introduce virtual vertices to account for the grain boundaries curvature. Second, to simplify this technique, the microstructure is mapped on hexagonal lattice sites, where each lattice site is assigned three Euler angles that represent the grain orientation at that lattice site. Triple points are easily represented between three neighbouring points with different orientations as shown in Fig. 1.

During grain growth, the grain structure undergoes topological transformations. In the case of the 2D growth process, two operations express elementary topological changes of the microstructure, i.e., (i) neighbour switching (Fig. 2a) and (ii) annihilation of a three-sided grain (Fig. 2b), which are

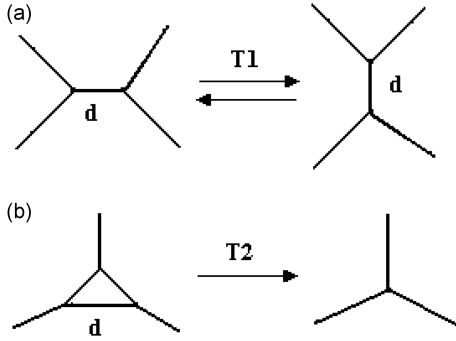


Fig. 2. Topological transformations: the neighbor switching (T1) (a) and annihilation of three-sided grain T2 (b).

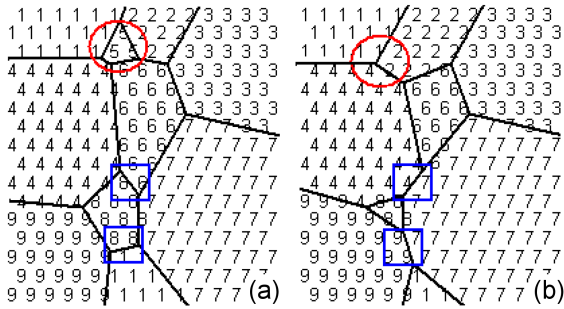


Fig. 3. Topological transformations using a hexagonal grid: T1 (in the blue squares), and T2 (in the red circle).

denoted T1 and T2, respectively. These two transformations are triggered when the distance between triple junctions is below a certain size. The challenge in the present study is how to make these transformations, and especially the T2 event.

In a T1 operation, neighbor switching occurs when the shrinking edge between two neighbouring vertices reaches a critical small length d_{th} . In Weygand's model [20], the length d is given by

$$d_{th} = \frac{\alpha}{n_{virt} + 1} \bar{R}, \quad (6)$$

where n_{virt} is the number of virtual vertices and α is a simulation parameter chosen small enough (0.025) to have a negligible influence on the grains size distribution.

In the present work, according to the hexagonal lattice sites, the smallest distance d corresponds to one in the blue squares (Fig. 3a) and is expressed by

$$d_{ex} = \frac{3}{2} \Delta, \quad (7)$$

where Δ is the spacing between lattice sites, i.e., the distance between two neighbouring lattice points.

In a T2 event, a triangular grain of a small area is eliminated, when one of its edges is shorter than some chosen critical value d . The vertex replaces the removed grain. The critical triangular grain is nearly equilateral and the value of d is equal to 5%

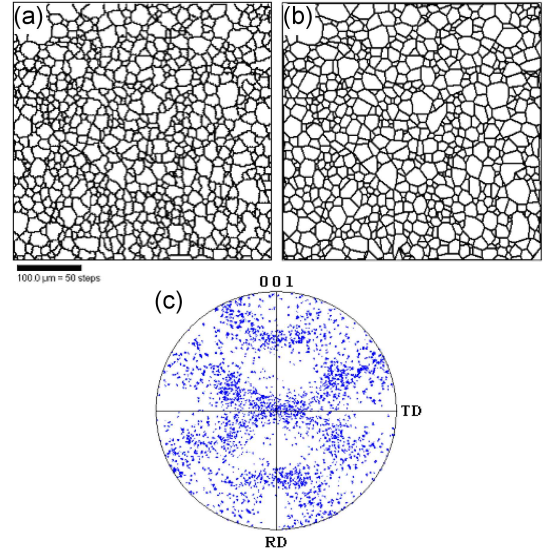


Fig. 4. Experimental microstructure characterized by EBSD (a), the corresponding network of lines (b), and the corresponding (001) pole figure (c).

of the initial average diameter [3]. In the present paper, the use of a hexagonal grid permits us to define the critical triangular grain that is equilateral containing 3 neighbouring lattice sites, as shown in the red circle (Fig. 3a). In this case, (7) gives d .

Using hexagonal lattice sites can solve several problems that are bound to the use of the standard vertex models. For example, one can mention three obstacles. First, the difficulty to detect topological changes while using a vertex model limits the massively parallel computations. The use of a regular grid is convenient mainly for large-scale simulations with low computational costs. Second, when the Zener drag effect on the grain boundaries is incorporated in the model, more complex topology changes are required [24]. To surmount this obstacle, particles can be introduced into the simulation as sites that have a special orientation. An individual particle may consist of a cluster of neighbouring sites. Third, the problem of nucleation should be dealt with which is necessary for the study of dynamic recrystallization [12]. Nucleation can be accomplished by introducing the nucleus into the matrix lattice sites with orientation numbers chosen from an appropriate set.

4. Results and discussion

The starting microstructure used in the simulation was the real microstructure Fe-3%Si ($400 \times 400 \mu\text{m}^2$) characterized by electron backscattering diffraction (EBSD) (Fig. 4a). This microstructure contains $N_0 = 816$ grains with an average grain size of $\bar{R}_0 = 7.53 \mu\text{m}$. The scan was carried out over a hexagonal grid of 200×231 points with a step size $\Delta = 2 \mu\text{m}$. From the EBSD measurements,

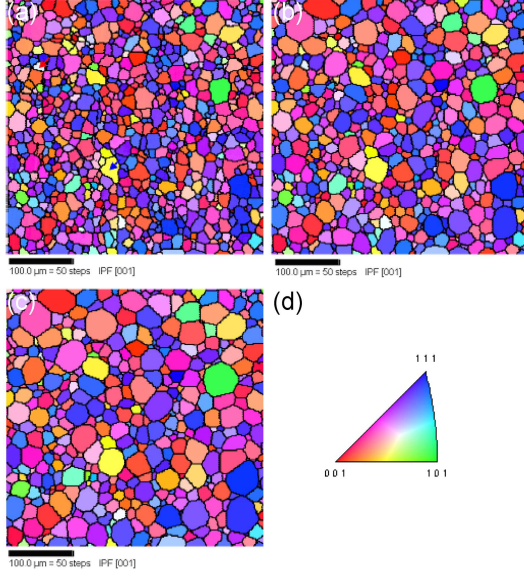


Fig. 5. Temporal evolution of the experimental microstructure at $t^* = 0$ (a), $t^* = 6$ (b), and $t^* = 15$ (c). Color code defined in the standard triangle (d).

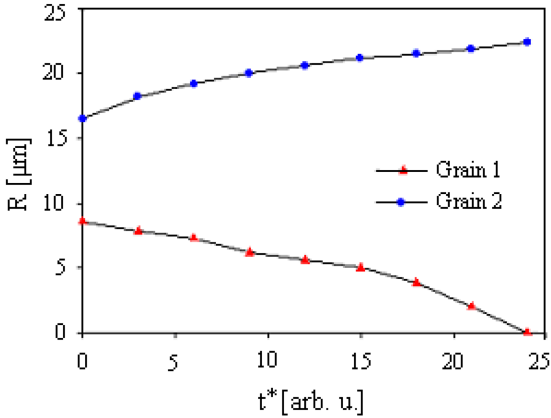


Fig. 6. Variation of grain size with time for the two grains 1 and 2.

every lattice point orientation is characterized by three Euler angles $(\varphi_1, \varphi, \varphi_2)$. The microstructure is reconstructed from these orientations. A grain is defined by neighbouring lattice points with the same orientation, i.e., when a disorientation angle between them less or equal to 2° . A grain boundary lies between two adjacent lattice points on the opposite side. Summing, both the network of lines or the network of grain boundaries and vertices at which these boundaries intersect can represent the microstructure. In Fig. 4b, grains are defined by the collection of boundaries and the triple junctions surrounding them. Analysis of the EBSD data is made by orientation imaging microscopy (OIMTM) to characterize the microstructure (grain size distribution, individual grain orientation, texture, inverse pole figure, and pole figure). Figure 4c shows the corresponding matrix (001) pole figure.

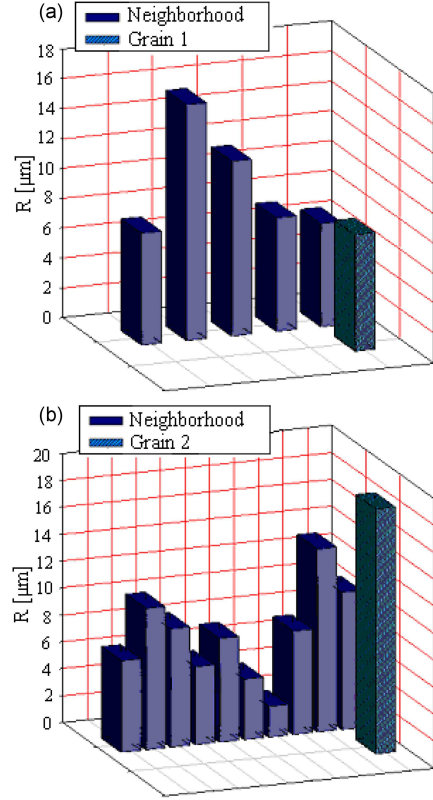


Fig. 7. Distribution in size and number of neighbouring grains for the two grains at $t^* = 3$.

According to (6) and using the present experimental data, the critical length given in the Weygand's model is $d = 0.19 \mu\text{m}$ in the case with no the virtual vertices ($n_{\text{virt}} = 0$) [20]. In the presence of the virtual vertices ($n_{\text{virt}} > 0$), the parameter d will be even smaller. On the other hand, $d = 0.38 \mu\text{m}$ from [3]. These values are very small at the mesoscopic scale, where the distance between two neighbouring sites is $\Delta = 2 \mu\text{m}$. Thus, it is reasonable to use in the simulation procedure the proposed experimental critical distance defined by (7), where $d_{ex} = 3 \mu\text{m}$.

In this paper, by using MATLAB software, the simulation is done for the isotropic case where all energies (σ) and mobilities (m) were assumed to be uniform. Normalized time is used

$$t = \frac{t^*}{m \sigma}. \quad (8)$$

The step time Δt is chosen to accurately describe the grain structure evolution. In the present work, Δt is defined as

$$\Delta t = \frac{3}{m \sigma}. \quad (9)$$

The microstructure's temporal evolution is displayed in Fig. 5. To pursue the local evolution of grains, orientation maps are used according to the color code defined in the unit triangle (Fig. 5d). At different stages of the simulation, normal grain growth occurs.

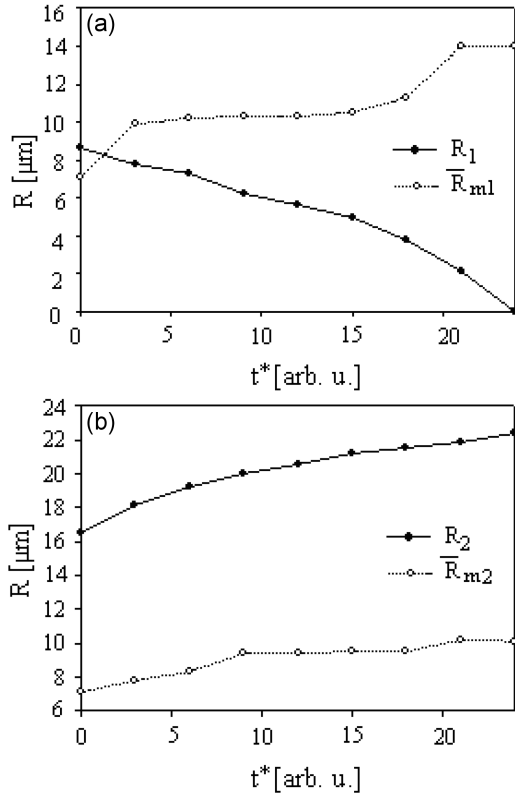


Fig. 8. Comparison between growth of the grains 1 and 2 and that of their first neighbors.

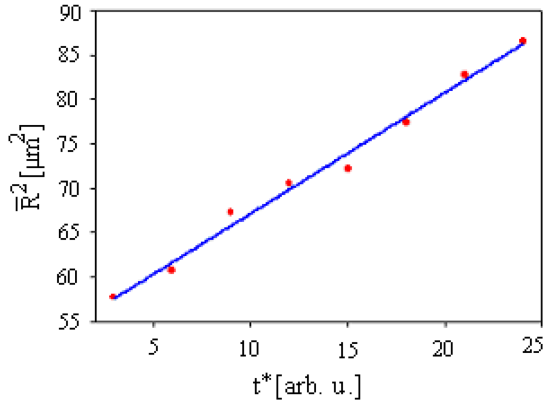


Fig. 9. Square mean-radius variation versus time.

Locally, the evolution of grain growth versus time is carried out for two grains noted “grain 1” and “grain 2”, respectively, with the red and blue arrows in Fig. 5a. In Fig. 6 one observes shrinking and vanishing of grain 1, and growing of grain 2.

Morphological and topological aspects of grain growth can be related to neighborhood behaviors [25], which is very difficult to explore using the standard vertex model. For example, Fig. 7 shows the neighborhood distribution in size and number for the two grains. Grain 1 with $n = 5$ will shrink (Fig. 7a), in turn, grain 2 with $n = 10$ will grow (Fig. 7b). This behavior is in good agreement with the von Neumann–Mullins law in (5).

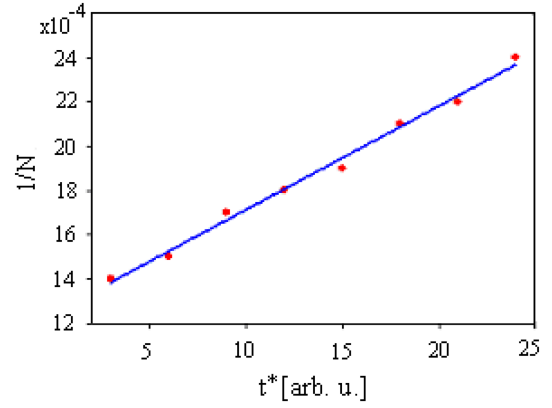


Fig. 10. Variation of reciprocal grains number with time.

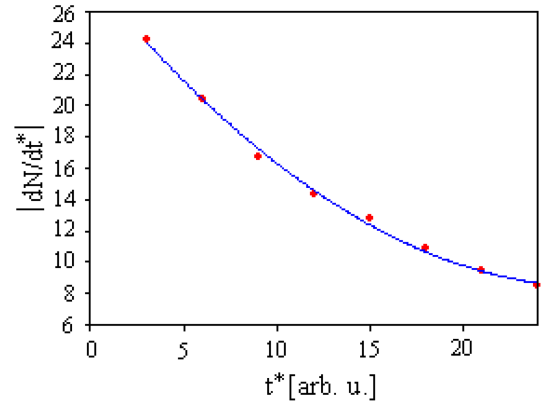


Fig. 11. Grain shrinkage velocity variation versus time.

The grain boundary ij between two neighbouring grains i and j with radii R_i and R_j , respectively, moves with the rate

$$\left(\frac{dR_i}{dt}\right)_j = c m_{gb} \sigma_{gb} \left(\frac{1}{R_j} - \frac{1}{R_i}\right), \quad (10)$$

where c is a dimensionless constant. For n neighbouring grains, the average growth rate of the i -th grain can be expressed by

$$\frac{dR_i}{dt} = c m_{gb} \sigma_{gb} \left(\frac{1}{\bar{R}_{mi}} - \frac{1}{R_i}\right), \quad (11)$$

where \bar{R}_{mi} is the neighbourhood average radius

$$\frac{1}{\bar{R}_{mi}} = \frac{1}{n} \sum_{j=1}^n \frac{1}{R_j}. \quad (12)$$

A grain with $R_i > \bar{R}_{mi}$ will grow, whereas a grain with $R_i < \bar{R}_{mi}$ will shrink. Figure 8 shows the evolution of R_i and \bar{R}_{mi} as a function of time for the two grains ($i = 1-2$).

Figure 9 illustrates the average matrix grain radius change over time. This result demonstrates that the square average grain size increases linearly with time in accordance with the parabolic kinetics in (4).

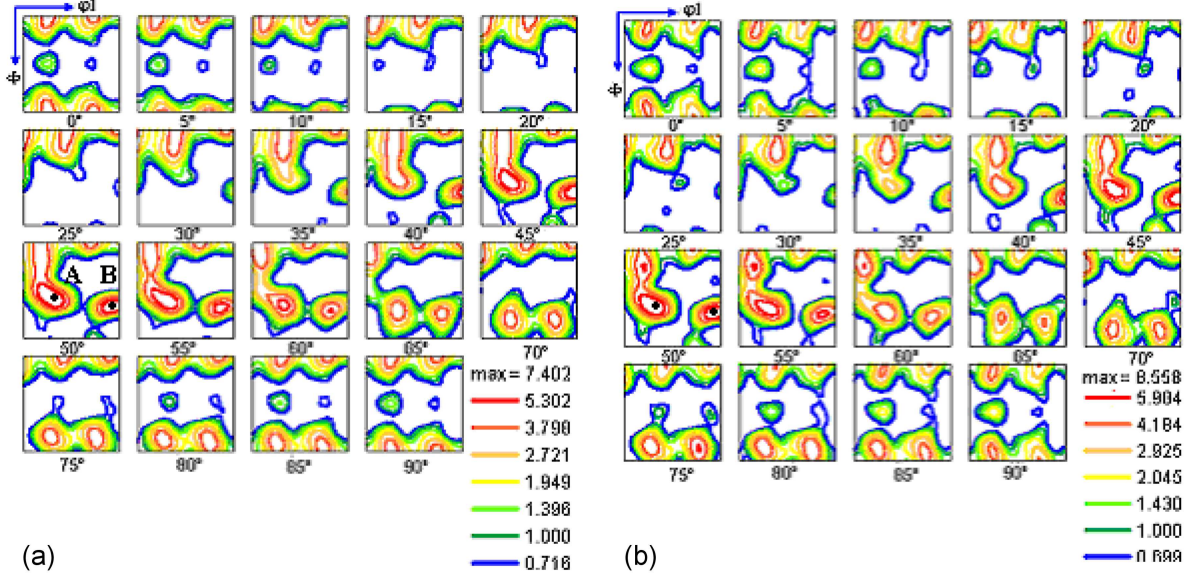


Fig. 12. Sections of ODF at φ_2 constant for $t^* = 0$ (a) and $t^* = 24$ (b).

Together with the circular grains hypothesis, the matrix average areas \bar{S}_0 and \bar{S} are respectively given by

$$\bar{S} = \pi \bar{R}^2 \quad \text{and} \quad \bar{S}_0 = \pi \bar{R}_0^2. \quad (13)$$

On the other hand, using the total matrix area S_T , the two matrix average areas are as follows

$$\bar{S} = \frac{S_T}{N} \quad \text{and} \quad \bar{S}_0 = \frac{S_T}{N_0}. \quad (14)$$

Substituting (13) and (14) into (4), the variation of grains number during grain growth process will be

$$\frac{1}{N} - \frac{1}{N_0} = \frac{\pi k t}{S_T}. \quad (15)$$

Topological events such as grain shrinkage can be expressed by changing the number of grains at each time step. Figure 10 depicts the time dependence of the reciprocal number of grains N . It was found that the number of grains decrease with simulation time. By linear fitting, one obtains a line

$$\frac{1}{N} = 4.68 \times 10^{-5} t^* + 1.24 \times 10^{-3}. \quad (16)$$

Note that (16) demonstrates that N decreases with time, which is consistent with (15). The grain shrinkage velocity can be expressed as

$$\frac{dN}{dt^*} = -4.68 \times 10^{-5} N^2. \quad (17)$$

The sign ($-$) indicates that N is decreasing. The number of grains decreases fast in the early stage of the simulation (Fig. 11) due to the presence of a large number of small grains that vanish during the grain growth process.

In pure single-phase polycrystalline material without particles, normal grain growth is a continuous process during which the grains grow uniformly. The grain growth and the evolution of the crystallographic texture during the annealing of materials are closely related. The texture development during

grain growth can be studied in terms of the orientation distribution function (ODF) intensities [26]. To see the evolution of the textural state at each step of the simulation process, the ODF's φ_2 sections have been calculated using the OIMTM maps. The texture change was analyzed for the two microstructures obtained at $t^* = 0$ and $t^* = 24$, respectively. Figure 12 shows the increase of the maximum ODF value from 7.4 at $t^* = 0$ (a) to 8.5 at $t^* = 24$ (b) due to normal grain growth. For example, from the sections $\varphi_2 = 50^\circ$, the maximum increases from 7.2 ($t^* = 0$) to 8.3 ($t^* = 24$) for the point A ($24.8^\circ, 50.9^\circ, 50^\circ$), and from 7.1 ($t^* = 0$) to 8.0 ($t^* = 24$) for the point B ($84.8^\circ, 60.0^\circ, 50.0^\circ$), respectively.

5. Conclusions

The observed difficulty, when one uses the standard vertex model, comes from the complexity of the representation of the microstructure and consequently the results analysis. In the present work, to take into account the microstructure morphological and textural inhomogeneities, the vertex method for the grain growth simulation was started with an experimental microstructure measured by electron backscattering diffraction (EBSD). To agree with the experiment data, a new representation of the microstructure has been proposed. Instead of using only the network of grain boundaries and vertices to represent the microstructure, the physical space is discretized on a regular grid of points where each point of the lattice is assigned three Euler angles that represent the grain orientation at that point. This modification improves the vertex simulation efficiency and reproduces the global features of the grain growth process.

References

- [1] J.E. Burke, D. Turnbull, *Prog. Metal Phys.* **3**, 220 (1952).
- [2] K. Kawasaki, T. Nagai, K. Nakashima, *Phil. Mag. B* **60**, 399 (1989).
- [3] A. Soares, A.C. Ferro, M.A. Fortes, *Scr. Metall.* **19**, 1491 (1985).
- [4] L.A. Barrales Mora, *Math. Comput. Sim.* **80**, 1411 (2010).
- [5] M.P. Anderson, D.J. Srolovitz, G.S. Grest, P.S. Sahni, *Acta Metall.* **32**, 783 (1984).
- [6] D.J. Srolovitz, G.S. Grest, M.P. Anderson, *Acta Metall.* **34**, 1833 (1986).
- [7] C.L.D. Prinzio, E. Druetta, O.B. Nasello, *Modell. Simul. Mater. Sci. Eng.* **21**, 025007 (2013).
- [8] M. Sitko, K. Banaś, L. Madej, *Materials* **14**, 4082 (2021).
- [9] S. Raghavan, S. Sahay, *Mater. Sci. Eng. A* **445–446**, 203 (2007).
- [10] Y. Liu, M. Militzer, M. Perez, *Materials* **12**, 4048 (2019).
- [11] J. Nandy, H. Sarangi, S. Sahoo, *Adv. Manuf.* **6**, 107 (2018).
- [12] Y. Mellbin, H. Hallberg, M. Ristinmaa, *Modelling Simul. Mater. Sci. Eng.* **23**, 045011 (2015).
- [13] Y. Mellbin, H. Hallberg, M. Ristinmaa, *Int. J. Sol. Struct.* **125**, 150 (2017).
- [14] L.A. Barrales Mora, G. Gottstein, L.S. Shvindlerman, *Acta Mater.* **60**, 546 (2012).
- [15] M. Syha, D. Weygand, *Mater. Sci. Forum* **715–716**, 563 (2012).
- [16] A. Harun, E.A. Holm, M.P. Clode, M.A. Miodownik, *Acta Mater.* **54**, 3261 (2006).
- [17] S.I. Wright, M.M. Nowell, *Microsc. Microanal.* **12**, 72 (2006).
- [18] B. L. Adams, S.I. Wright, K. Kunze, *Metall. Trans. A.* **24A**, 819 (1993).
- [19] K. Fuchizaki, T. Kusaba, K. Kawasaki, *Phil. Mag. B* **71**, 333 (1995).
- [20] D. Weygand, Y. Bréchet, *Phil. Mag. B* **78**, 329 (1998).
- [21] M. Hillert, *Acta Metall.* **13**, 227 (1965).
- [22] J. von Neumann, *J. Metall. Interfaces*, 108 (1952).
- [23] W.W. Mullins, *J. Appl. Phys.* **27**, 900 (1956).
- [24] D. Weygand, Y. Bréchet, J. Lepinoux, *Acta mater.* **47**, 961(1999).
- [25] N. Maazi, *Comput. Mater. Sci.* **79**, 303 (2013).
- [26] M. Yasuda, T. Kataoka, Y. Ushigami, K. Murakami, K. Ushioda, *ISIJ Inter.* **58**, 1893 (2018).